Journal of the American Heart Association

ORIGINAL RESEARCH

# Inhibiting Succinate Release Worsens Cardiac Reperfusion Injury by Enhancing Mitochondrial Reactive Oxygen Species Generation

Alexander S. Milliken, M.Sc.; Sergiy M. Nadtochiy, PhD; Paul S. Brookes, PhD

**BACKGROUND:** The metabolite succinate accumulates during cardiac ischemia. Within 5 minutes of reperfusion, succinate returns to baseline levels via both its release from cells and oxidation by mitochondrial complex II. The latter drives reactive oxygen species (ROS) generation and subsequent opening of the mitochondrial permeability transition (PT) pore, leading to cell death. Targeting succinate dynamics (accumulation/oxidation/release) may be therapeutically beneficial in cardiac ischemia–reperfusion (IR) injury. It has been proposed that blocking MCT1 (monocarboxylate transporter 1) may be beneficial in IR injury, by preventing succinate release and subsequent engagement of downstream inflammatory signaling pathways. In contrast, herein we hypothesized that blocking MCT1 would retain succinate in cells, exacerbating ROS generation and IR injury.

**METHODS AND RESULTS:** Using the mitochondrial ROS probe mitoSOX and a custom-built murine heart perfusion rig built into a spectrofluorometer, we measured ROS generation in situ during the first moments of reperfusion. We found that acute MCT1 inhibition enhanced mitochondrial ROS generation at reperfusion and worsened IR injury (recovery of function and infarct size). Both of these effects were abrogated by tandem inhibition of mitochondrial complex II, suggesting that succinate retention worsens IR because it drives more mitochondrial ROS generation. Furthermore, using the PT pore inhibitor cyclosporin A, along with monitoring of PT pore opening via the mitochondrial membrane potential indicator tetramethylrhodamine ethyl ester, we herein provide evidence that ROS generation during early reperfusion is upstream of the PT pore, not downstream as proposed by others. In addition, pore opening was exacerbated by MCT1 inhibition.

**CONCLUSIONS:** Together, these findings highlight the importance of succinate dynamics and mitochondrial ROS generation as key determinants of PT pore opening and IR injury outcomes.

**Key Words:** complex II ■ ischemia ■ metabolism ■ mitochondria ■ reactive oxygen species ■ succinate

The metabolite succinate has a central role in tissue ischemia. Several mechanisms exist for ischemic succinate accumulation,[1,2] and this process is conserved across diverse tissues, species, and physiologic contexts.[3,4] However, rapid oxidation of accumulated succinate at the onset of tissue reperfusion is a key event in ischemia–reperfusion (IR) injury, the underlying pathology of myocardial infarction (heart attack).[1,2] This has led to intense interest in succinate as a potential therapeutic target.[5–9]

Approximately one-third of succinate accumulated during ischemia is rapidly oxidized by mitochondrial complex II (Cx-II) of the mitochondrial respiratory chain.[2,10] This leads to the generation of reactive oxygen species (ROS) via mechanisms that are thought to involve either reverse electron transport at Cx-I[11–13] or

Correspondence to: Paul S. Brookes, PhD, FAHA, Department of Anesthesiology and Perioperative Medicine, Box 604, University of Rochester Medical Center, 601 Elmwood Avenue, Rochester, NY 14642. Email: paul_brookes@urmc.rochester.edu

Preprint posted on BioRxiv April 27, 2022. doi: https://doi.org/10.1101/2022.04.27.489760.

Supplemental Material is available at https://www.ahajournals.org/doi/suppl/10.1161/JAHA.121.026135

For Sources of Funding and Disclosures, see page 14.



*JAHA* is available at: www.ahajournals.org/journal/jaha

## CLINICAL PERSPECTIVE

### What Is New?

- A new method has been developed for simultaneous measurement of both cardiac function and small-molecule probe fluorescence (reactive oxygen species and mitochondrial membrane potential) in the perfused mouse heart.
- Acutely blocking succinate release via MCT1 (monocarboxylate transporter 1) worsens ischemia–reperfusion injury by exacerbating reactive oxygen species generation during the first minute of reperfusion in a manner that can be abrogated by tandem blockade of succinate oxidation by mitochondrial complex II.
- Characterization of the kinetics of the mitochondrial permeability transition pore relative to reactive oxygen species generation reveals that reactive oxygen species lie upstream of the pore, not downstream as others have proposed.

### What Are the Clinical Implications?

- Although inhibition of MCT1 may confer cardioprotection in vivo by preventing extracellular succinate from engaging inflammatory signaling, our data suggest inhibiting MCT1 may worsen acute injury by exacerbating damage from intracellular succinate in early reperfusion.
- Because the detrimental effects of MCT1 inhibitors are abrogated by mitochondrial complex II inhibition, optimal therapy for ischemia–reperfusion injury should incorporate both complex II and MCT1 inhibitors to deal with the consequences of both intracellular and extracellular succinate, respectively.
- Despite recent clinical trial failures, these basic science data advocate continued interest in the therapeutic potential of the permeability transition pore inhibitor cyclosporin A for ischemia–reperfusion injury.

### Nonstandard Abbreviations and Acronyms

| | |
|---|---|
| **AA5** | atpenin A5 |
| **AR** | AR-C155858 |
| **CsA** | cyclosporin A |
| **Cx** | mitochondrial complex |
| **DMM** | dimethyl malonate |
| **IR** | ischemia–reperfusion |
| **$\lambda_{EM}$** | emission wave length |
| **$\lambda_{EX}$** | excitation wavelength |
| **MCT1** | monocarboxylate transporter 1 |
| **NADH** | nicotinamide adenine dinucleotide reduced form |
| **NAD(P)H** | NADH and nicotinamide adenine dinucleotide phosphate reduced forms |
| **PT** | permeability transition |
| **ROS** | reactive oxygen species |
| **S1QEL** | suppressor of site $I_Q$ electron leak |
| **SUCNR1** | succinate receptor 1 |
| **TMRE** | tetramethylrhodamine ethyl ester |
| **$\Delta\Psi_m$** | mitochondrial membrane potential |

forward electron transport at Cx-III.[14–18] Mitochondrial ROS generation potentiates opening of the mitochondrial permeability transition (PT) pore,[19–22] which triggers necrotic cell death.

The remaining two-thirds of succinate accumulated during ischemia is released upon reperfusion, in a pH-dependent manner via MCT1 (monocarboxylate transporter 1).[10,23] The physiologic function of this released succinate is unclear, with suggestions that it may serve as a metabolic signal of hypoxia.[24] Succinate is a ligand for the widely expressed SUCNR1 (succinate receptor 1, formerly orphan G protein coupled receptor 91, GPR91), which elicits a range of physiologic responses.[25] Most relevant to IR injury, SUCNR1 signaling promotes inflammation via macrophage activation, which may contribute to the pathology of IR injury.[10,26–30] As such, it has been postulated that inhibiting MCT1 would be beneficial in IR injury, via blunting of extracellular succinate ➔ SUCNR1 signaling.[10,31]

In contrast, given the key role of intracellular succinate for ROS generation during reperfusion, we hypothesized herein that acute blockade of succinate release via MCT1 would worsen IR injury, and that simultaneous blockade of Cx-II would abrogate this effect. This hypothesis was tested by measuring mitochondrial ROS generation in situ in perfused mouse hearts using a custom-built perfusion rig within the chamber of a benchtop spectrofluorometer. In addition, because it has been proposed that PT pore opening itself may lie upstream of the burst of ROS seen upon reperfusion,[23,32] we used this apparatus to interrogate the temporal relationship between ROS generation and PT pore opening during early reperfusion.

## METHODS

All original data used to prepare the figures are available in spreadsheet form on the data-sharing website FigShare (https://doi.org/10.6084/m9.figshare.19319627). All methods used are as detailed below, with further information and materials or other resources available from the authors upon request.

## Animals and Reagents

Animal and experimental procedures complied with the National Institutes of Health *Guide for Care and Use of Laboratory Animals* (8th Edition, 2011) and were approved by the University of Rochester Committee on Animal Resources (protocol number 2007–087). Male and female C57BL/6J adult mice (8–20 weeks old) were housed in a pathogen-free vivarium with 12-hour light–dark cycles and food and water ad libitum. Mice were administered terminal anesthesia via intraperitoneal 2,2,2-tribromoethanol (Avertin) ≈250 mg/kg. Avertin was prepared in amber glass vials and stored at 4 °C for not >1 month. This agent was chosen for anesthesia because it does not impact cardioprotection as reported for volatile anesthetics or opioids[33–35] and does not have mitochondrial depressant effects as reported for barbiturates.[36] Euthanizing occurred via cardiac extirpation (see below).

MitoSOX red was from Thermo (NJ) and was stored aliquoted under argon before use. Fully oxidized mitoSOX was prepared by reaction with Fremy salt as described elsewhere.[37] AR-C155858 (AR) was from MedChemExpress (Monmouth Junction, NJ). Unless otherwise stated, all other reagents were from MilliporeSigma (St. Louis, MO).

## Perfused Mouse Hearts

Following establishment of anesthetic plane (toe-pinch response), beating mouse hearts were rapidly cannulated, excised, and retrograde perfused at a constant flow (4 mL/min) with Krebs-Henseleit buffer consisting of (in millimoles per liter): NaCl (118), KCl (4.7), $MgSO_4$ (1.2), $NaHCO_3$ (25), $KH_2PO_4$ (1.2), $CaCl_2$ (2.5), glucose (5), pyruvate (0.2), lactate (1.2), and palmitate (0.1, conjugated 6:1 to bovine serum albumin). Krebs-Henseleit buffer was gassed with 95% $O_2$ and 5% $CO_2$ at 37 °C. A water-filled balloon connected to a pressure transducer was inserted into the left ventricle and expanded to provide a diastolic pressure of 6 to 8 mm Hg. Cardiac function was recorded digitally at 1 kHz (Dataq, Akron, OH) for the duration of the protocol. Following equilibration (10–20 minutes) IR injury comprised 25 minutes. Global no-flow ischemia plus 60 minutes. Reperfusion. Hearts were then sliced and stained with triphenyltetrazolium chloride for infarct quantitation by planimetry (red=live tissue, white=infarct). Infarction analysis was blinded to experimentalists.

The following conditions (Figure 1F) were examined: (1) Control: DMSO vehicle infusion 5 minutes before ischemia and 5 minutes into reperfusion. (2) S1QEL: Suppressor of site $I_Q$ electron leak 1.1: 1.6 µmol/L, delivered 5 minutes before ischemia and 5 minutes into reperfusion. (3) DMM5: Dimethyl malonate (DMM), 5 mmol/L at the onset of reperfusion and 5 minutes into reperfusion. (4) AR: MCT1 inhibitor AR-C155858 (AR), 10 µmol/L infusion 5 minutes before ischemia and 5 minutes into reperfusion. (5) AR+DMM5: 10 µmol/L AR infusion 5 minutes before ischemia and 5 minutes into reperfusion, plus 5 mmol/L DMM at the onset of reperfusion and 5 minutes into reperfusion. (6) AR+DMM10: 10 µmol/L AR infusion 5 minutes before ischemia and 5 minutes into reperfusion plus 10 mmol/L DMM at the onset of reperfusion and 5 minutes into reperfusion. (7) AR+AA5: 10 µmol/L AR infusion 5 minutes before ischemia and 5 minutes into reperfusion plus 100 nmol/L atpenin A5 (AA5) at the onset of reperfusion and 5 minutes into reperfusion. (8) CsA: 0.8 µmol/L cyclosporin A (CsA) infusion[38] 5 minutes before ischemia and 5 minutes into reperfusion. Simultaneously with these conditions, hearts were delivered either 1.5 µmol/L mitoSOX for 5 minutes or 500 nmol/L tetramethylrhodamine ethyl ester (TMRE) for 20 minutes before ischemia.

## Perfusion Apparatus Within Spectrofluorometer

A cardiac perfusion apparatus was custom built with an umbilicus to position the heart within the light-proof enclosure of a Varian/Cary Eclipse benchtop spectrofluorometer (Agilent, Santa Clara, CA), as shown in Figure 1A through 1C. Hearts were placed against the wall of a water-jacketed cuvette maintained at 37 °C in which the excitation light source strikes the left ventricle of the heart at a 45° angle relative to the photomultiplier tube window. The cuvette holder was 3-dimensionally printed (the .stl file is available upon request). Data were collected using Cary WinUV Kinetics software, which permitted real-time fluorescence monitoring (1-second reads/15-second cycle, photomultiplier tube voltage 600, Ex/Em slit width=5 nm) for the duration of the perfusion protocol. At the heart rates observed (mean±SD, 438±54 bpm; N=54) a 1 second fluorescent read was averaged across approximately 7 heart beats, so gating for motion artifacts was unnecessary. Initial validation was performed by monitoring endogenous NAD(P)H fluorescence ($\lambda_{EX}$ 340 nm, $\lambda_{EM}$ 460 nm) and flavoprotein fluorescence ($\lambda_{EX}$ 460 nm, $\lambda_{EM}$ 520 nm), as shown in Figure 1D and 1E.

## Measuring In Situ Mitochondrial ROS

Mitochondrial ROS generation was measured using the probe mitoSOX[39,40] (triphenylphosphonium-conjugated dihydroethidium) at a concentration of 1.5 µmol/L, because the triphenylphosphonium moiety is known to uncouple mitochondria at concentrations ≥2.5 µmol/L.[41–43] Hearts subject to conditions 1 to 7 described above were equilibrated for 10 minutes, loaded with 1.5 µmol/L mitoSOX for 5 minutes, and then immediately subjected to 25 minutes ischemia.

Fluorescence was monitored at $\lambda_{EX}$ 510 nm and $\lambda_{EM}$ 580 nm.

Because the $\lambda_{EX}$ and $\lambda_{EM}$ of mitoSOX overlap with the absorbance spectra of endogenous chromophores in cardiomyocytes (eg, myoglobin and cytochromes), changes in chromophore absorbance during the course of IR could impact the fluorescent signal. Furthermore, the distribution of the mitoSOX probe between cytosolic and mitochondrial matrix compartments is determined by the mitochondrial membrane potential ($\Delta\Psi_m$), which would also be expected to change during IR. To

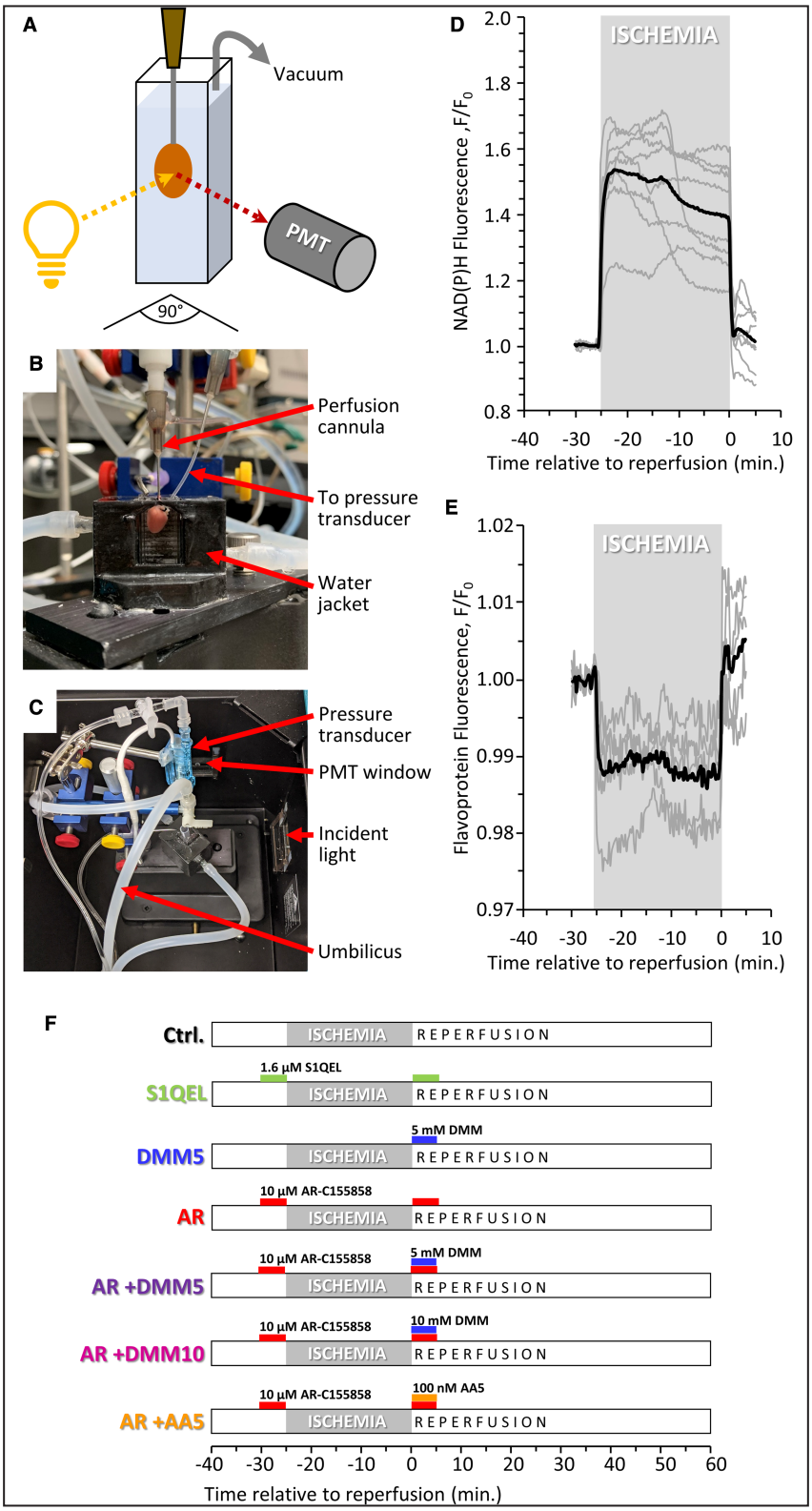

**Figure 1. Fluorescence cardiac perfusion system.**
**A**, Schematic showing arrangement of the perfused mouse heart relative to light source and photomultiplier tube (PMT). **B**, Photograph of heart in situ before mounting inside spectrofluorometer. **C**, Photograph of cardiac perfusion apparatus from above mounted inside spectrofluorometer. Components of the system are labeled, including a custom 3-dimensionally printed water-jacketed cuvette holder, heated umbilical lines to deliver Krebs-Henseleit buffer at 37 °C to the heart, and vacuum line to remove perfusate/effluent. **D**, Nicotinamide adenine dinucleotide phosphate (NAD[P]H) autofluorescence (340/460 nm) during ischemia and reperfusion. Traces in gray are individual hearts, with the average (N=7) shown in black. **E**, Flavoprotein autofluorescence (462/520 nm) during ischemia and reperfusion. Traces in gray are individual hearts, with the average (N=4) shown in black. Fluorescence data are normalized to preischemic levels. **F**, Schematic showing design of the 7 experimental perfusion conditions examined herein. Where indicated, suppressor of site $I_Q$ electron leak 1.1 (S1QEL1.1) (mitochondrial complex [Cx]-I reactive oxygen species inhibitor), dimethylmalonate (DMM; Cx-II inhibitor), AR-C155858 (AR; MCT1 [monocarboxylate transporter 1] inhibitor), or atpenin A5 (AA5; Cx-II inhibitor) were administered at the listed concentrations. Colors and terms used to denote each condition are used throughout the remainder of the figures.

correct for these potential cofounding effects, a series of hearts were loaded with fully oxidized mitoSOX[37] that fluoresces in a manner that is independent of ROS generation, but is still subject to the effects of chromophore absorbance and probe distribution. Fluorescent data from these hearts were used to correct data obtained with naïve mitoSOX (conditions 1–7), yielding a net signal that originated only from in situ probe oxidation, without contribution from other factors. The data process for this correction is illustrated in Figure S1, which also shows a minimal change in signal during IR when no mitoSOX was present. In addition, absorbance spectra of compounds tested in this study (eg, AR, DMM, S1QEL) were also measured to ensure these chemicals did not absorb significant amounts of light at the $\lambda_{EX}$ and $\lambda_{EM}$ of mitoSOX (Figure S2).

## Measuring In Situ $\Delta\Psi_m$

To assess the timing of mitochondrial PT pore opening, mitochondrial membrane potential was measured using TMRE at 500 nmol/L delivered for 20 minutes before ischemia. The PT pore inhibitor CsA (0.8 µmol/L) was optionally delivered for 5 minutes before ischemia. To determine changes upon reperfusion, TMRE data were normalized to the fluorescent signal during the last 5 minutes of ischemia. Two conditions were examined: control IR and IR with MCT1 inhibition (same as condition 7 above). Attempts to determine the effect of CsA on PT pore opening in the presence of AR were confounded by interactions between these molecules and TMRE, resulting in precipitation of components in Krebs-Henseleit buffer.

## Effluent Analysis by High-Performance Liquid Chromatography

Effluents from control and AR-treated hearts were collected in 1-minute intervals for the first 3 minutes of reperfusion and immediately treated with 10% perchloric acid. Following addition of 100 nmols butyrate as an internal standard, samples were frozen in liquid $N_2$ and stored at −80 °C until analysis. Samples were centrifuged at 20 000*g* to remove insoluble materials. Metabolites were resolved on high-performance liquid chromatography (Shimadzu [Kyoto, Japan] Prominence 20 system) using two 300×7.8 mm Aminex HPX-87H columns (BioRad, Carlsbad, CA) in a series with 10 mmol/L $H_2SO_4$ mobile phase (flow rate: 0.7 mL/min) and a 100-µL sample injected on the column. Succinate and lactate were detected using a photodiode array measuring absorbance at 210 nm as previously described.[2] A standard curve was constructed for calibration. Lactate data were corrected for 1.2 mmol/L lactate contained in the Krebs-Henseleit buffer.

## Statistical Analysis

Comparisons between the 2 groups were made using unpaired Student *t* tests. For multiple group comparisons, ANOVA was used with post hoc Tukey honest significant difference tests. Data are shown as mean±SEM. Numbers of biological replicates are noted in the figures. Significance was set at α=0.05.

# RESULTS

## Cardiac Fluorescence

Although similar spectrofluorometric cardiac perfusion apparatus has previously been constructed,[32,44–48] prior efforts have used larger animal hearts (rats, guinea pigs) or have not simultaneously measured cardiac function. To the best of our knowledge, this is the first study of mouse hearts with simultaneous fluorescence and functional assessment.

The spectrofluorimetric perfusion system was first validated by monitoring NAD(P)H and flavoprotein autofluorescence during ischemia and reperfusion (Figure 1D and 1E). As expected, NADPH ($\lambda_{EX}$ 340 nm, $\lambda_{EM}$ 460 nm) autofluorescence immediately rose upon ischemia, in agreement with previous reports.[32,44,49,50] Likewise, flavoprotein fluorescence ($\lambda_{Ex}$ 460 nm, $\lambda_{Em}$ 520 nm) decreased upon ischemia.[32,50,51] Both parameters returned to baseline levels immediately upon reperfusion.

NAD(P)H autofluorescence in the heart is thought to mainly represent mitochondrial NADH, the substrate for Cx-I, which accumulates during ischemia because of a highly reduced respiratory chain.[50] The

mitochondrial ATP synthase is thought to operate in reverse during ischemia to maintain $\Delta\Psi_m$,[52,53] and this also contributes to feedback inhibition of Cx-I, resulting in high NADH.[11] Notably, a decrease in NAD(P)H signal was observed approximately 12 minutes into ischemia, concurrent with the onset of ischemic hypercontracture (not shown). The latter is thought to indicate the onset of an energetic crisis (no ATP to relax contractile machinery).[54]

## mitoSOX Fluorescence

Having validated the cardiac fluorescence system, we next sought to use it for measurement of ROS generation during IR. Figure 2A shows cardiac functional measurements throughout IR (heart rate×pressure product), whereas Figure 2B shows the corrected mitoSOX fluorescent readout over the same period.

To account for changes in the absorbance of endogenous chromophores during IR, or probe distribution, additional hearts were perfused with oxidized mitoSOX or with no probe at all. No significant change in the fluorescent signal was observed in hearts without mitoSOX (Figure S1A). However, delivery of oxidized mitoSOX resulted in a rapid increase in the fluorescent signal during dye loading (Figure S1B). At the onset of ischemia, an additional signal increase was seen. This is expected, because it has been shown that cardiac tissue absorbance at 510 and 580 nm decreases during ischemia.[55] Upon reperfusion, after a small increase, the oxidized mitoSOX signal steadily declined for the remainder of the experiment. This is possibly because of loss of the dye from mitochondria as a result of changes in $\Delta\Psi_m$ as mitochondrial integrity becomes compromised.

Raw mitoSOX fluorescence traces (Figure S1C) also increased slightly during loading, but not to the same extent as the fully oxidized probe. A sharp signal increase at the onset of ischemia may represent a burst of ROS generation as the terminal respiratory chain becomes inhibited. Upon reperfusion, a sustained signal increase was observed for ≈10 minutes, followed by a decline. Using the oxidized mitoSOX data to correct the raw mitoSOX data, Figure 2B (Figure S1D) shows the signal resulting from oxidation of the probe during IR. Upon reperfusion, a sustained increase in the redox-dependent mitoSOX signal was seen, and this is consistent with the concept that a burst of mitochondrial ROS generation occurs during the first minutes of reperfusion.[1,56–58]

It has been posited that reverse electron transport at Cx-I is the primary source of ROS during reperfusion, and recently, a novel series of inhibitors that target ROS generation at the ubiquinone (Q) binding site of Cx-I (termed S1QELs) were shown to elicit cardioprotection against IR injury.[59] Succinate levels return to baseline within the first 5 minutes of reperfusion,[2] and accordingly, examining mitoSOX fluorescence during this time period revealed that the immediate signal increase at the onset of reperfusion in control hearts was suppressed in hearts treated with a S1QEL (Figure 3A through 3C). These data suggest that the ROS signal detected by mitoSOX during the first minutes of reperfusion originates from Cx-I reverse electron transport. However, by 2 minutes, the rate of signal increase in

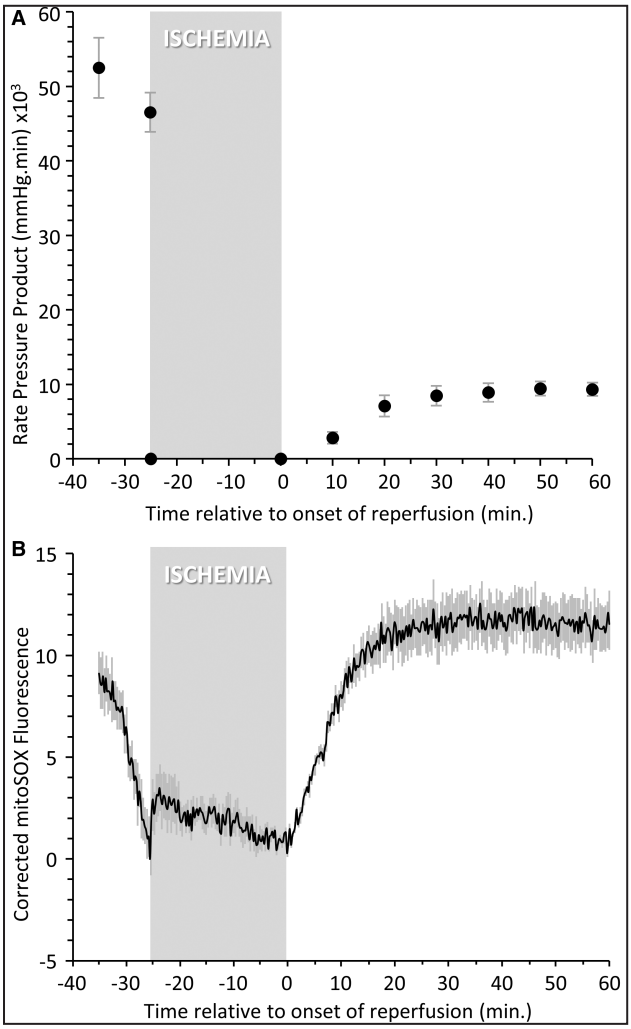


**Figure 2. Cardiac function vs mitoSOX fluorescence during ischemia–reperfusion (IR).**
**A**, Cardiac functional measurements. Graph shows heart rate×left ventricular developed pressure (ie, rate pressure product) for the period of 25 minutes. Ischemia is indicated. Data are mean±SEM, N=16. **B**, Corrected mitoSOX fluorescence (510/580 nm) during IR. Fluorescent data were processed as described in the Methods section and as shown in Figures S1 through S5, to correct for changes in absorbance of endogenous cytochromes at the fluorescence wavelengths. Data are mean±SEM, N=6. MitoSOX fluorescent measurements were not performed for the entire perfusion time for all hearts in (**A**) (eg, some hearts were used for controls or other measurements), hence the different N between panels.

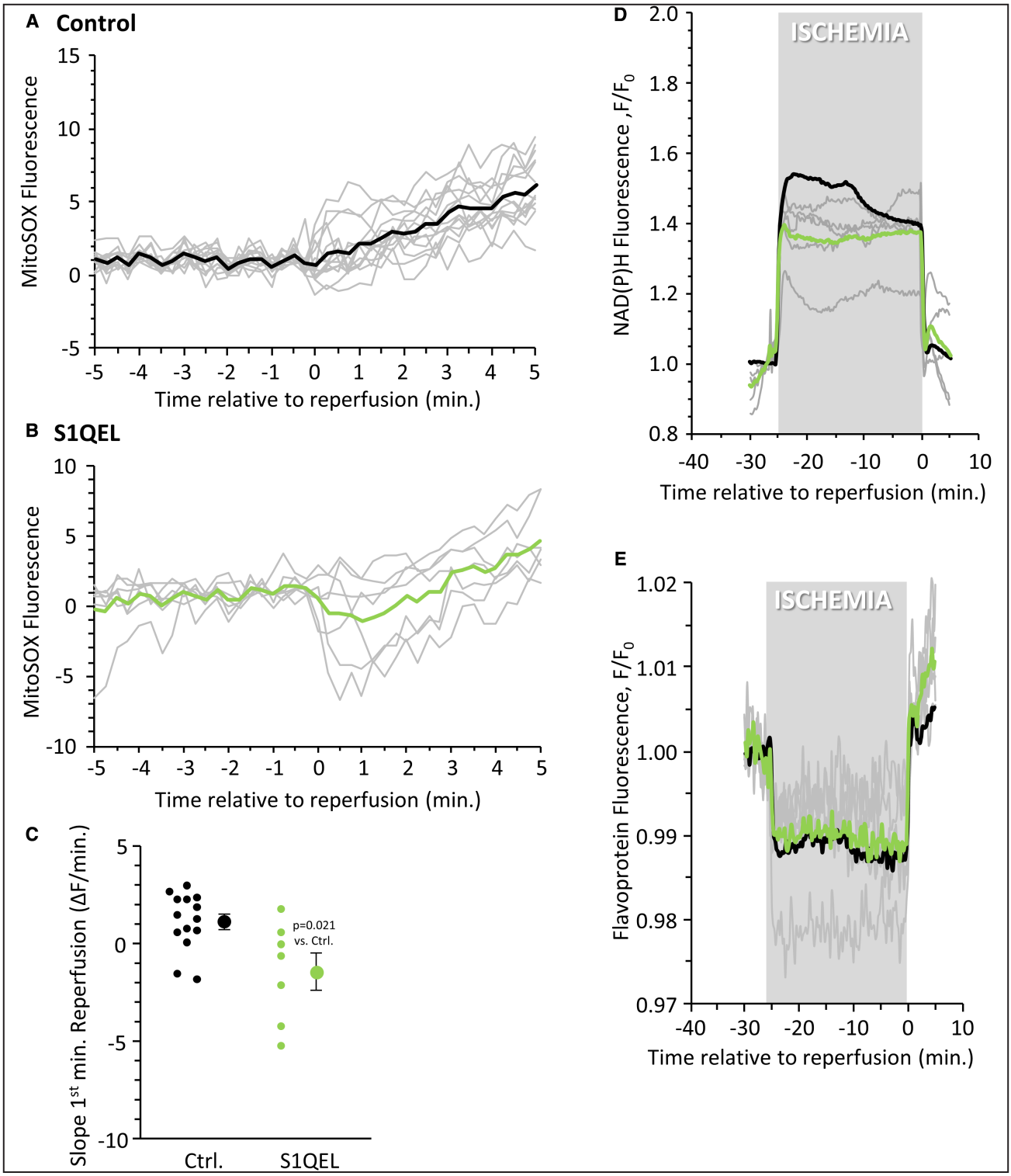


**Figure 3. Impact of suppressor of site $I_Q$ electron leak (S1QEL) on ischemia–reperfusion (IR) injury dynamics.**
Hearts were treated with the mitochondrial complex I Q-site reactive oxygen species generation inhibitor S1QEL1.1 for 5 minutes pre- and postischemia (Figure 1 schematic). **A**, Control mitoSOX fluorescent data during the first 5 minutes of reperfusion (from Figure 2B) for comparative purposes. **B**, mitoSOX fluorescent data from S1QEL-treated hearts. Gray traces show individual data, with averages shown as a bold line. **C**, Calculated slopes from the first minute of reperfusion, for the data in (**A** and **B**). For each condition, individual data points are shown on the left, with mean±SEM on the right (N for each condition can be seen from the number of data points). *P* values (ANOVA followed by unpaired Student *t* test) for differences between groups are denoted. **D**, Nicotinamide adenine dinucleotide phosphate (NAD(P)H autofluorescence (340/460 nm) during IR. Traces in gray are individual hearts, with the average (N=5) shown in green. **E**, Flavoprotein autofluorescence (462/520 nm) during ischemia and reperfusion. Traces in gray are individual hearts, with the average (N=5) shown in green. **D** and **E**, Average data from control hearts (from Figure 1) are shown in black for comparative purposes. Fluorescence data are normalized to preischemic levels. Ctrl. indicates control.

S1QEL hearts had returned to that seen in control hearts, potentially indicating a role for other sources of ROS.[17] Although no effect of S1QEL on flavoprotein fluorescence was observed (Figure 3E), S1QEL did cause a slight detriment in the elevation of NAD(P)H fluorescence at the start of ischemia (37±4% with S1QEL versus 53±5% in controls, $P$=0.042). However, it also blunted the NAD(P)H response to ischemic hypercontracture (Figure 3D). The combination of these effects was such that the drop in NAD(P)H signal at the onset of reperfusion was not significantly different between S1QEL versus control (30±4% versus 36±4%, respectively), suggesting that consumption of NADH by Cx-I during early reperfusion was not impacted by the compound.

## Preventing Succinate Efflux Exacerbates Mitochondrial ROS at Reperfusion

Upon reperfusion of ischemic heart, one-third of accumulated succinate is oxidized by Cx-II, driving ROS generation.[2,10] Consistent with this, the Cx-II competitive inhibitor malonate is reported to be cardioprotective when delivered at reperfusion.[6,7,60] The remaining two-thirds of succinate accumulated during ischemia is released from tissue upon reperfusion, and the pathway for this release was recently elucidated as MCT1.[2,10] To test the impact of MCT1 inhibition on ROS generation at reperfusion, hearts were infused peri-ischemically with the MCT1 inhibitor AR,[61] which resulted in a significant decrease in succinate release into the postcardiac effluent during the first 3 minutes of reperfusion (Figure S3). As expected, lactate efflux was also significantly diminished, confirming MCT1 inhibition.

Figure 4C and 4F show that AR resulted in a significantly greater rate of ROS generation during the first minute of reperfusion compared with control. To investigate the requirement for Cx-II in the additional AR-induced mitoSOX signal, the competitive Cx-II inhibitor DMM (5 mmol/L) was used. Surprisingly, DMM alone at this concentration did not significantly impact the mitoSOX signal, and it also did not significantly blunt the additional signal induced by AR (Figure 4B, 4D, and 4F). We hypothesized that because malonate is a competitive Cx-II inhibitor, it may not be able to outcompete the additional succinate present in cells caused by MCT1 inhibition. Supporting this hypothesis, tandem administration of a higher dose of DMM (10 mmol/L) was capable of blocking the elevated mitoSOX signal elicited by AR, returning it to control levels (Figure 4E and 4F). Furthermore, the potent Cx-II inhibitor AA5 (100 nmol/L) was also effective in blocking the additional mitoSOX signal induced by AR (Figure S4A and S4B). Overall, these data suggest that MCT1 inhibition enhances mitochondrial ROS generation in the first minute of reperfusion, in a manner that can be blocked by inhibitors of Cx-II.

## Blocking Succinate Release Via MCT1 Worsens IR Injury

In agreement with the role of succinate-derived ROS as a driver of post-IR pathology, DMM alone improved and AR worsened IR injury (Figure 5A through 5C), although these effects were only significant in terms of infarct size while failing to reach significance (Tukey honest significant difference test) for functional recovery. In addition, tandem administration of low-dose (5 mmol/L) or high-dose (10 mmol/L) DMM reversed the impact of AR. Furthermore, administration of the potent Cx-II inhibitor AA5 also blocked the impact of AR on functional recovery and infarct (Figure S4C through S4E) and was more protective than AA5 alone.[2] These effects of MCT1 inhibition and Cx-II inhibition were more significant for myocardial infarction (Figure 5C) than for functional recovery (Figure 5B), but all trended in the same direction, similar to mitoSOX data (Figure 4) (ie, interventions that increased mitoSOX signal at reperfusion worsened IR injury, and those that decreased it improved IR injury). Overall, a correlation was observed between the effect of interventions on mitoSOX at reperfusion and on infarct size and functional recovery, as illustrated in Figure 6.

## Timing of Mitochondrial ROS at Reperfusion Versus PT Pore Opening

Although it is largely accepted that ROS can trigger PT pore opening, it has also been proposed that during reperfusion injury, the PT pore itself may drive ROS generation.[23,32] To test this, we measured the effect of the PT pore inhibitor CsA on mitoSOX fluorescence during reperfusion. CsA was chosen at 0.8 µmol/L, because this was previously shown to elicit protection in mouse hearts.[38] As shown in Figure 7B and 7C, CsA had no impact on mitoSOX fluorescence during reperfusion. To confirm that PT pore opening did occur, hearts were loaded with the $\Delta\Psi_m$ indicator TMRE. Upon reperfusion, an immediate rise in TMRE fluorescence was observed. Subsequently, in control hearts the TMRE signal declined from approximately 5 minutes into reperfusion, whereas in CsA-treated hearts, the signal was sustained (Figure 7D and 7E). We thus infer that PT pore opening occurs no sooner than 5 minutes into reperfusion. Despite a small blip in the mitoSOX signal in control hearts at approximately 6.5 minutes, no substantial difference was seen between control and CsA hearts at this time point, concurrent with divergence of the TMRE traces, thus suggesting no secondary ROS burst because of PT pore opening.

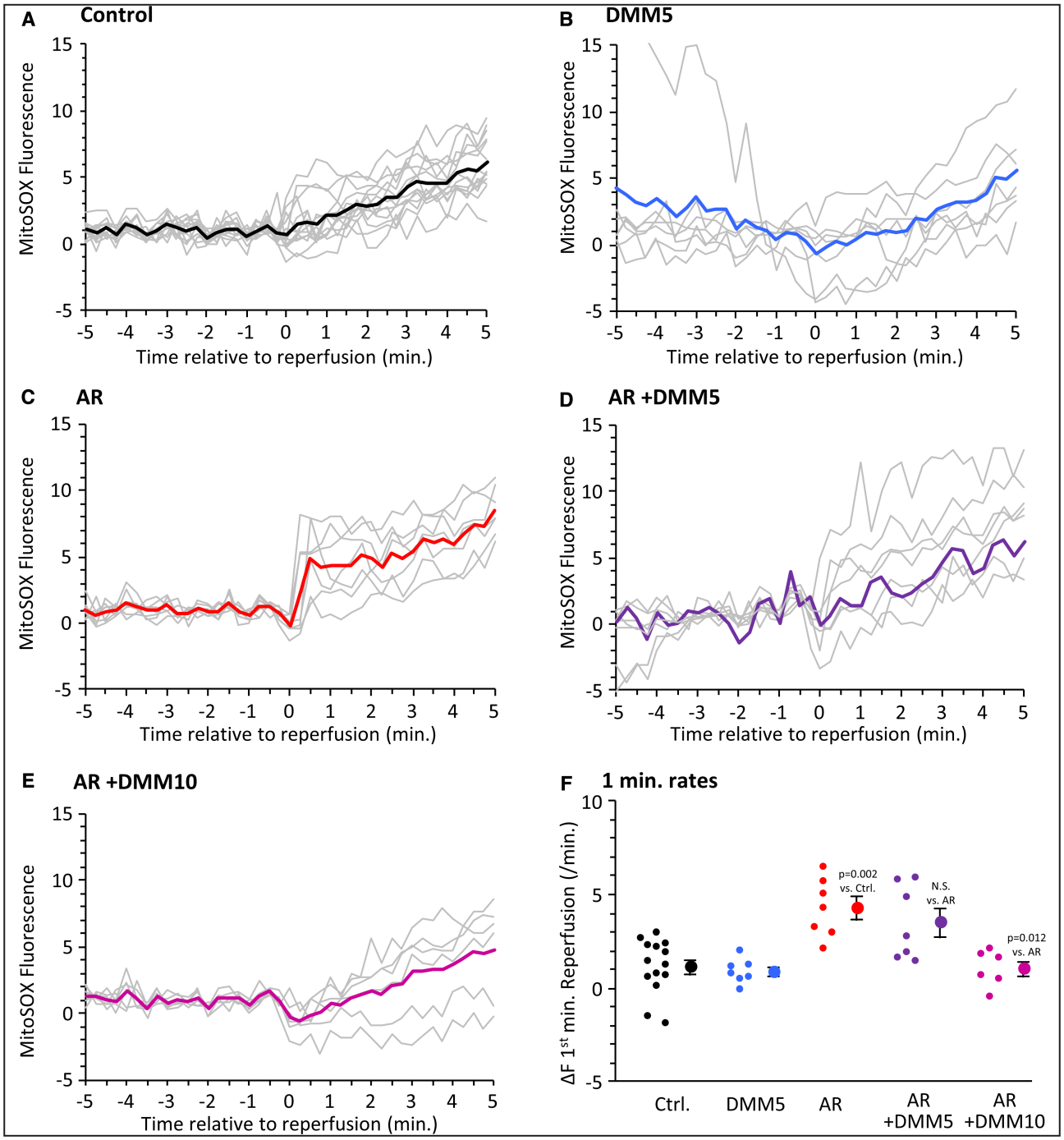


**Figure 4. Impact of AR-C155858 (AR) and mitochondrial complex II inhibitors on mitoSOX fluorescence at reperfusion.** **A** through **E**, Corrected mitoSOX traces 5 minutes pre- and postreperfusion for the labeled conditions. Gray traces are individual data, with averages shown as bold colored lines (see Figure 1 for color scheme). **F**, Calculated slopes from first minute of reperfusion for the data in (**A** through **E**). For each condition, individual data points are shown on the left, with mean±SEM on the right (N for each condition can be seen from the number of data points). *P* values (ANOVA followed by Tukey honest significant difference test) for differences between groups are denoted. Ctrl. indicates control; DMM, dimethyl malonate; and N.S., not significant.

Finally, as expected from its impact on mitoSOX fluorescence during early reperfusion (Figure 4), inhibition of MCT1 led to an accelerated loss of the TMRE signal during reperfusion, indicating faster opening of the PT pore (Figure S5).

## DISCUSSION

Cardiac IR is a complex pathology, with numerous links between early and late events in the development of myocardial infarction. Shortly after reperfusion, a

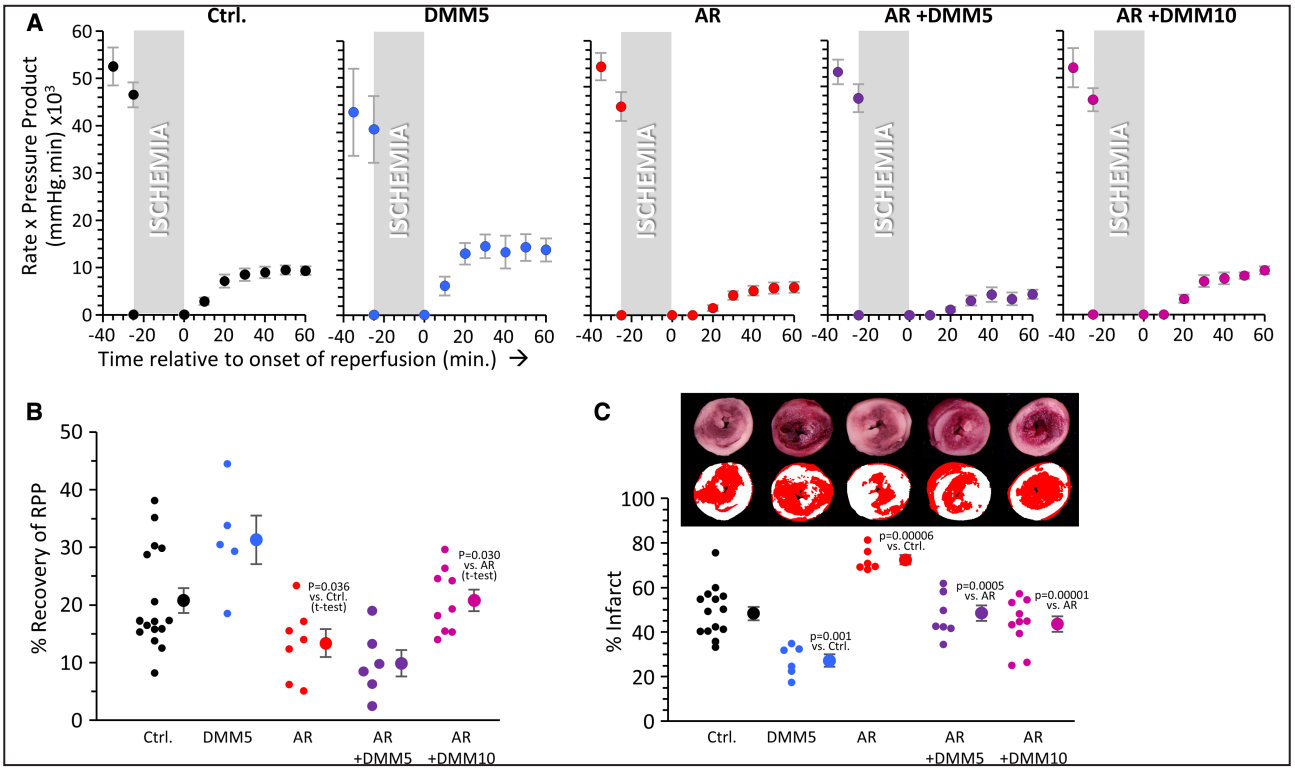


**Figure 5. Impact of AR-C155858 (AR) and mitochondrial complex II inhibitors on outcomes of ischemia–reperfusion (IR) injury.**

**A**, Cardiac functional measurements during IR. Graphs show heart rate×left ventricular developed pressure (ie, rate pressure product [RPP]) for each of the conditions examined for the period of 25 minutes ischemia is indicated. Data are mean±SEM. **B**, Quantitation of percent functional recovery (ie, cardiac function at 60 minutes of reperfusion as a percentage of that immediately before ischemia [–25 minutes time point]). For each condition, individual data points are shown on the left, with mean±SEM shown on the right (N for each condition can be seen from number of data points). No significant differences were observed between groups by ANOVA followed by Tukey honest significant difference (HSD) test, although *P* values from ANOVA followed by unpaired Student *t* test did denote differences between groups as shown above the data. **C**, Myocardial infarct size for each condition. Images above the graph show representative triphenyltetrazolium chloride–stained heart cross-sections, with pseudocolored mask used for planimetry below. Graph shows data for each condition, with individual data points on the left and mean±SEM on the right (N for each condition can be seen from number of data points). *P* values (ANOVA followed by Tukey HSD test) for differences between groups are denoted above the data. Ctrl. indicates control; DMM, dimethyl malonate; and N.S., not significant.

burst of ROS generation and mitochondrial $Ca^{2+}$ overload both trigger opening of the mitochondrial PT pore, a key event in necrotic cell death of cardiomyocytes. Following this, inflammatory cells (macrophages, neutrophils) are recruited to the heart, where they mediate responses that lead to cardiac remodeling, fibrosis, and eventual development of hypertrophy and heart failure.[62–64]

Accumulation of succinate in hypoxia/ischemia is highly conserved,[3,4] but this succinate drives ROS generation upon tissue reperfusion, and this has led to a consensus that intracellular succinate plays a detrimental role in reperfusion injury.[1,2,16,65,66] In contrast, succinate release from cells via MCT1,[2,10,23] along with the recent identification of a succinate receptor (GPR91/SUCNR1[25]), have led to the notion that extracellular succinate may also play a role in IR.[6,10] In this regard, findings from an in vivo model of cardiac IR injury demonstrated that blocking succinate release via MCT1 was cardioprotective, likely because of inhibiting immune system activation.[6,10] However, herein our data reveal that acutely blocking MCT1 in a perfused heart system (where there are no inflammatory cells) leads to greater ROS generation and the worsening of IR injury. Reconciling these findings, it is possible that MCT1 inhibition is detrimental in the acute setting at the level of cardiomyocytes, but this is balanced in vivo by a longer-term effect of MCT1 inhibition, possibly involving receptor-mediated succinate effects on other cell types, including inflammatory cells. Together, these studies highlight that the therapeutic targeting of MCT1 may require careful timing and titration to balance detrimental versus beneficial effects of blocking succinate release.

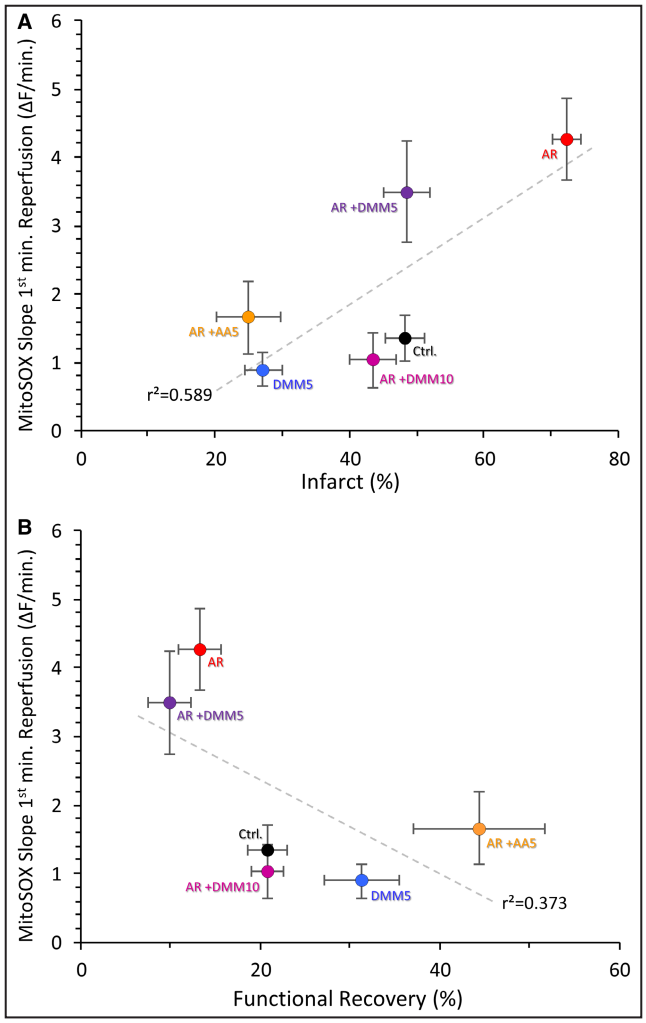


**Figure 6. Correlations between mitoSOX fluorescence during reperfusion and ischemia–reperfusion outcomes.** Graphs show correlation between mitoSOX slope data and (**A**) infarct size or (**B**) functional recovery. Each data point is the mean±SEM for a condition (see color scheme in Figure 1). mitoSOX data are from Figure 3F and Figure S5B. Infarct data are from Figure 4C and Figure S4E. Functional data are from Figure 4B and Figure S4C. Linear curve fits are shown, with correlation coefficient ($r^2$) listed alongside. AR indicates AR-C155858; Ctrl., control; and DMM, dimethyl malonate.

Inhibiting MCT1 in the heart lowered succinate release into the effluent by approximately 30%. Assuming this succinate was retained in cells and available for oxidation by Cx-II, it is therefore not surprising that MCT1 inhibition also led to enhanced ROS generation. Furthermore, although 5 mmol/L of the competitive Cx-II inhibitor malonate was ineffective at blocking this additional ROS, doubling its concentration to 10 mmol/L effectively overrode the impact of AR. Unfortunately, because of the physical nature of dimethylmalonate (liquid) and our drug infusion system, it was not possible to test additional even higher doses of DMM. Instead, we tested the potent Cx-II inhibitor AA5 ( $IC_{50}$10 nmol/L[67]), and found that it was able to completely abrogate the additional ROS induced by AR, and this resulted in cardioprotection to a level greater than baseline control IR injury (Figure S4). The combination of AR and AA5 may be considered optimal from a therapeutic perspective, keeping succinate inside cells to prevent its signaling effects and preventing its oxidation to generate ROS.

Although there is a general consensus that mitochondrial ROS generation during early reperfusion is an upstream event that triggers PT pore opening, it has also been suggested that pore opening itself is the main driver of ROS generation in early reperfusion.[23,32] Our results (Figure 7) suggest that the burst of ROS at reperfusion is independent of the PT pore, because evidence for pore opening (ie, a CsA-sensitive loss of $\Delta\Psi_m$) was not observed until at least 5 minutes into reperfusion, by which time a large amount of ROS generation had already occurred.

It should not go unmentioned that $Ca^{2+}$ is also considered to be a major trigger for PT pore opening,[68,69] with both $Ca^{2+}$ and ROS thought to potentiate each other's effects at promoting pore formation.[70] Thus, future experiments should be directed at using fluorescent $Ca^{2+}$ probes in this or similar perfusion systems to understand in situ $Ca^{2+}$ kinetics and how they relate to ROS and pore-opening kinetics in early reperfusion.

Several caveats on the use of mitoSOX as a probe for mitochondrial ROS should be addressed. First, it is known the probe can be oxidized by reactants other than ROS, although notably, 1-electron oxidations result in nonfluorescent products that would be undetectable in our measurement system.[71] Furthermore, the mitoSOX signal increase in early reperfusion was inhibited by S1QEL, a specific inhibitor of ROS generation at Cx-I,[59] so we consider any contribution from other poorly characterized oxidation sources to be minimal. Second, the mitoSOX signal is impacted both by its distribution between extracellular, cytosolic, and mitochondrial compartments,[37] and by the primary and secondary filter effects from endogenous chromophores[47,55] (see Methods section). However, our use of fully oxidized mitoSOX as a control (Figure S1) ensures that any changes in the mitoSOX signal we observed originated only from in situ probe oxidation, and not from redistribution of the probe or changes in the absorbance of myoglobin or cytochromes.

Although mitoSOX does confer limitations on the assignment of the signal to a particular ROS, similar issues of probe specificity are also broadly applicable to genetically encoded biosensors.[72,73] In addition, more precise analytical methods, such as liquid-chromatography mass spectrometry (LC–MS) separation of mitoSOX oxidation products,[37,74] require time-consuming isolation steps that may release components that further oxidize the probe during isolation, and therefore may not be readily compatible with the

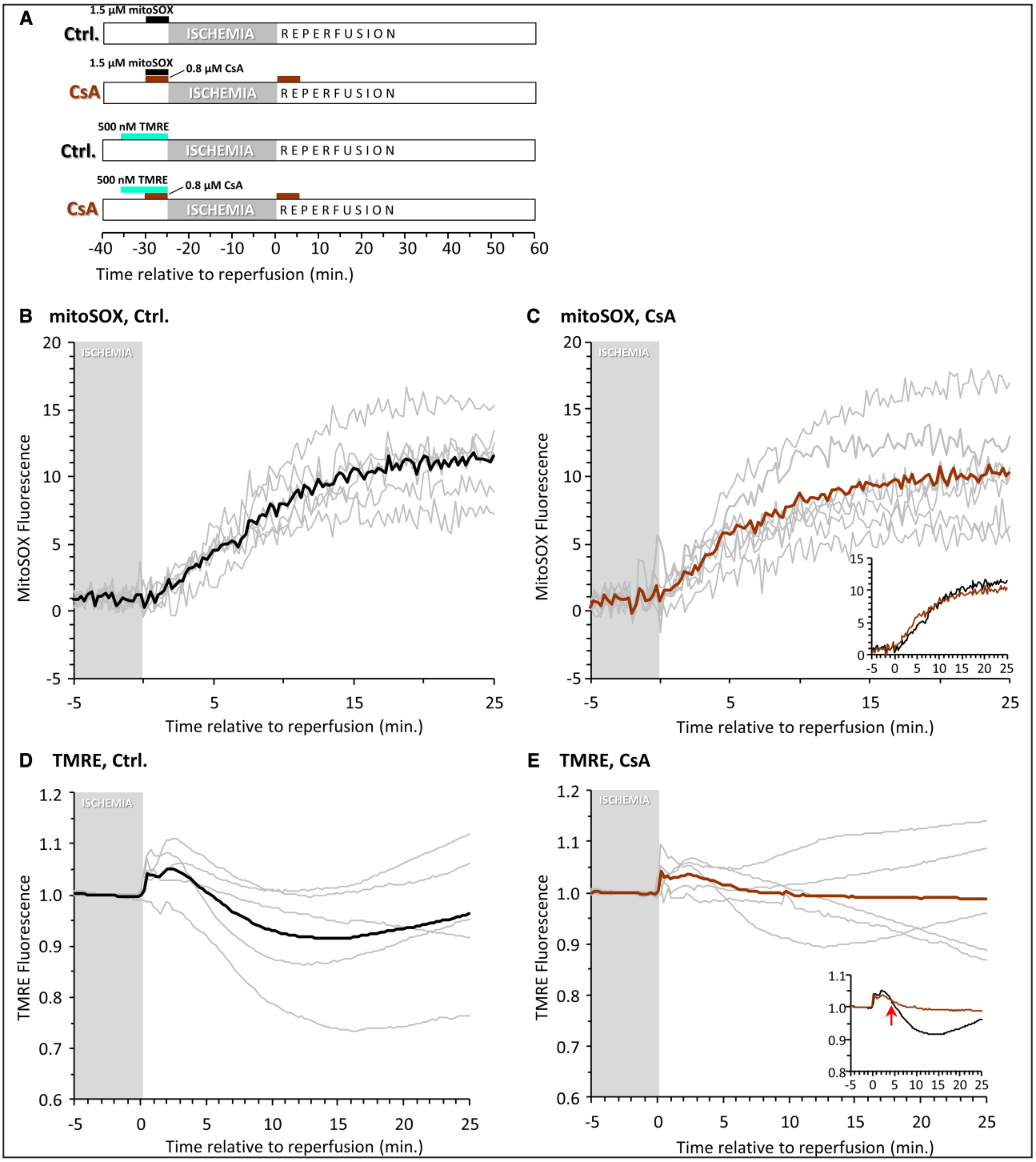


**Figure 7. Temporal relationship between mitoSOX and permeability transition (PT) pore opening during ischemia–reperfusion.**

**A**, Schematic showing perfusion conditions. Where indicated, mitoSOX (reactive oxygen species indicator), tetramethylrhodamine ethyl ester (TMRE) (mitochondrial membrane potential indicator) and/or cyclosporin A (CsA) (PT pore inhibitor) were administered at the listed concentrations. **B** and **C**, mitoSOX signal during early reperfusion under control (Ctrl.) or CsA condition. The last 5 minutes of the ischemic period is indicated. Gray traces show individual data, with averages shown as bold lines. Inset to (**C**) shows averages for control and CsA superimposed. **D** and **E**, Normalized TMRE fluorescence during early reperfusion under control or CsA condition. The last 5 minutes of the ischemic period is indicated. Gray traces show individual data, with averages shown as bold lines. Inset to (**C**) shows averages for control and CsA superimposed. Red arrow indicates the point at which traces diverge 5 minutes into reperfusion.

rapid kinetics of the events observed herein. The development of more precise genetically encoded and non–$\Delta\Psi_m$-dependent mitochondrial ROS probes may therefore be useful in future studies.

Overall, the findings herein demonstrate that blocking MCT1 in cardiac IR leads to inhibition of succinate release, which worsens IR injury because of enhanced mitochondrial ROS generation. Concurrent inhibition of Cx-II abrogates these effects, highlighting the importance of succinate oxidation at Cx-II in the pathology of IR injury. Furthermore, these events appear to lie temporally upstream of PT pore opening. Future experiments could explore the role of local succinate signaling in the heart to determine if SUCNR1 may modulate responses to IR in a manner independent of inflammatory cells, providing further insight on the delicate balance of succinate dynamics in IR injury.

## ARTICLE INFORMATION

Received March 15, 2022; accepted May 26, 2022.

### Affiliations

Department of Pharmacology and Physiology (A.S.M.), and Department of Anesthesiology and Perioperative Medicine (S.M.N., P.S.B.), University of Rochester Medical Center, Rochester, NY

### Acknowledgments

The authors thank R. S. Balaban (National Heart, Lung, and Blood Institute) for constructive discussions on corrections for primary and secondary filtering effects during early design stages of this project.

Author contributions: A. S. Milliken and Dr Brookes designed the research. A. S. Milliken and Dr Nadtochiy performed the experiments. A. S. Milliken and Dr Brookes analyzed the data and wrote the article. All authors approved the final version of the article.

### Sources of Funding

This work was supported by a grant from the National Institutes of Health (R01-HL071158). A. S. Milliken is funded by an American Heart Association Predoctoral Fellowship (number 21PRE829767) and formerly National Institutes of Health T32-GM068411.

### Disclosures

None.

### Supplemental Material

Figures S1–S5

## REFERENCES

1. Chouchani ET, Pell VR, Gaude E, Aksentijevic D, Sundier SY, Robb EL, Logan A, Nadtochiy SM, Ord ENJ, Smith AC, et al. Ischaemic accumulation of succinate controls reperfusion injury through mitochondrial ROS. *Nature*. 2014;515:431–435. doi: 10.1038/nature13909
2. Zhang J, Wang YT, Miller JH, Day MM, Munger JC, Brookes PS. Accumulation of succinate in cardiac ischemia primarily occurs via canonical Krebs cycle activity. *Cell Rep*. 2018;23:2617–2628. doi: 10.1016/j.celrep.2018.04.104
3. Hochachka PW, Dressendorfer RH. Succinate accumulation in man during exercise. *Eur J Appl Physiol Occup Physiol*. 1976;35:235–242. doi: 10.1007/BF00423282
4. Hochachka PW, Owen TG, Allen JF, Whittow GC. Multiple end products of anaerobiosis in diving vertebrates. *Comp Biochem Physiol B*. 1975;50:17–22. doi: 10.1016/0305-0491(75)90292-8
5. Pell VR, Chouchani ET, Frezza C, Murphy MP, Krieg T. Succinate metabolism: a new therapeutic target for myocardial reperfusion injury. *Cardiovasc Res*. 2016;111:134–141. doi: 10.1093/cvr/cvw100
6. Kula-Alwar D, Prag HA, Krieg T. Targeting succinate metabolism in ischemia/reperfusion injury. *Circulation*. 2019;140:1968–1970. doi: 10.1161/CIRCULATIONAHA.119.042791
7. Valls-Lacalle L, Barba I, Miro-Casas E, Ruiz-Meana M, Rodriguez-Sinovas A, Garcia-Dorado D. Selective inhibition of succinate dehydrogenase in reperfused myocardium with intracoronary malonate reduces infarct size. *Sci Rep*. 2018;8:2442. doi: 10.1038/s41598-018-20866-4
8. Pell VR, Chouchani ET, Murphy MP, Brookes PS, Krieg T. Moving forwards by blocking back-flow: the yin and yang of MI therapy. *Circ Res*. 2016;118:898–906. doi: 10.1161/CIRCRESAHA.115.306569
9. Chouchani ET, Pell VR, James AM, Work LM, Saeb-Parsy K, Frezza C, Krieg T, Murphy MP. A unifying mechanism for mitochondrial superoxide production during ischemia-reperfusion injury. *Cell Metab*. 2016;23:254–263. doi: 10.1016/j.cmet.2015.12.009
10. Prag HA, Gruszczyk AV, Huang MM, Beach TE, Young T, Tronci L, Nikitopoulou E, Mulvey JF, Ascione R, Hadjihambi A, et al. Mechanism of succinate efflux upon reperfusion of the ischaemic heart. *Cardiovasc Res*. 2021;117:1188–1201. doi: 10.1093/cvr/cvaa148
11. Lambert AJ, Brand MD. Superoxide production by NADH:Ubiquinone oxidoreductase (complex I) depends on the pH gradient across the mitochondrial inner membrane. *Biochem J*. 2004;382:511–517. doi: 10.1042/BJ20040485
12. Watson MA, Wong HS, Brand MD. Use of S1QELs and S3QELs to link mitochondrial sites of superoxide and hydrogen peroxide generation to physiological and pathological outcomes. *Biochem Soc Trans*. 2019;47:1461–1469. doi: 10.1042/BST20190305
13. Wong HS, Monternier PA, Brand MD. S1QELs suppress mitochondrial superoxide/hydrogen peroxide production from site IQ without inhibiting reverse electron flow through Complex I. *Free Radic Biol Med*. 2019;143:545–559. doi: 10.1016/j.freeradbiomed.2019.09.006
14. Cadenas E, Boveris A, Ragan CI, Stoppani AO. Production of superoxide radicals and hydrogen peroxide by NADH-ubiquinone reductase and ubiquinol-cytochrome c reductase from beef-heart mitochondria. *Arch Biochem Biophys*. 1977;180:248–257. doi: 10.1016/0003-9861(77)90035-2
15. Turrens JF, Alexandre A, Lehninger AL. Ubisemiquinone is the electron donor for superoxide formation by complex III of heart mitochondria. *Arch Biochem Biophys*. 1985;237:408–414. doi: 10.1016/0003-9861(85)90293-0
16. Murphy MP. How mitochondria produce reactive oxygen species. *Biochem J*. 2009;417:1–13. doi: 10.1042/BJ20081386
17. Chen Q, Vazquez EJ, Moghaddas S, Hoppel CL, Lesnefsky EJ. Production of reactive oxygen species by mitochondria: central role of complex III. *J Biol Chem*. 2003;278:36027–36031. doi: 10.1074/jbc.M304854200
18. Chen Q, Moghaddas S, Hoppel CL, Lesnefsky EJ. Ischemic defects in the electron transport chain increase the production of reactive oxygen species from isolated rat heart mitochondria. *Am J Physiol Cell Physiol*. 2008;294:C460–C466. doi: 10.1152/ajpcell.00211.2007
19. Morciano G, Giorgi C, Bonora M, Punzetti S, Pavasini R, Wieckowski MR, Campo G, Pinton P. Molecular identity of the mitochondrial permeability transition pore and its role in ischemia-reperfusion injury. *J Mol Cell Cardiol*. 2015;78:142–153. doi: 10.1016/j.yjmcc.2014.08.015
20. Bernardi P, Di Lisa F. The mitochondrial permeability transition pore: molecular nature and role as a target in cardioprotection. *J Mol Cell Cardiol*. 2015;78:100–106. doi: 10.1016/j.yjmcc.2014.09.023
21. Beutner G, Alavian KN, Jonas EA, Porter GA Jr. The mitochondrial permeability transition pore and ATP synthase. *Handb Exp Pharmacol*. 2017;240:21–46. doi: 10.1007/164_2016_5
22. Halestrap AP, Richardson AP. The mitochondrial permeability transition: a current perspective on its identity and role in ischaemia/reperfusion injury. *J Mol Cell Cardiol*. 2015;78:129–141. doi: 10.1016/j.yjmcc.2014.08.018
23. Andrienko TN, Pasdois P, Pereira GC, Ovens MJ, Halestrap AP. The role of succinate and ROS in reperfusion injury—a critical appraisal. *J Mol Cell Cardiol*. 2017;110:1–14. doi: 10.1016/j.yjmcc.2017.06.016
24. Reddy A, Bozi LHM, Yaghi OK, Mills EL, Xiao H, Nicholson HE, Paschini M, Paulo JA, Garrity R, Laznik-Bogoslavski D, et al. pH-gated succinate secretion regulates muscle remodeling in response to exercise. *Cell*. 2020;183:62–75.e17. doi: 10.1016/j.cell.2020.08.039

25. He W, Miao FJ, Lin DC, Schwandner RT, Wang Z, Gao J, Chen JL, Tian H, Ling L. Citric acid cycle intermediates as ligands for orphan G-protein-coupled receptors. *Nature*. 2004;429:188–193. doi: 10.1038/nature02488
26. Tannahill GM, Curtis AM, Adamik J, Palsson-McDermott EM, McGettrick AF, Goel G, Frezza C, Bernard NJ, Kelly B, Foley NH, et al. Succinate is an inflammatory signal that induces IL-1beta through HIF-1alpha. *Nature*. 2013;496:238–242. doi: 10.1038/nature11986
27. Trauelsen M, Hiron TK, Lin D, Petersen JE, Breton B, Husted AS, Hjorth SA, Inoue A, Frimurer TM, Bouvier M, et al. Extracellular succinate hyperpolarizes M2 macrophages through SUCNR1/GPR91-mediated Gq signaling. *Cell Rep*. 2021;35:109246. doi: 10.1016/j.celrep.2021.109246
28. Wu JY, Huang TW, Hsieh YT, Wang YF, Yen CC, Lee GL, Yeh CC, Peng YJ, Kuo YY, Wen HT, et al. Cancer-derived succinate promotes macrophage polarization and cancer metastasis via succinate receptor. *Mol Cell*. 2020;77:213–227.e215. doi: 10.1016/j.molcel.2019.10.023
29. van Diepen JA, Robben JH, Hooiveld GJ, Carmone C, Alsady M, Boutens L, Bekkenkamp-Grovenstein M, Hijmans A, Engelke UFH, Wevers RA, et al. SUCNR1-mediated chemotaxis of macrophages aggravates obesity-induced inflammation and diabetes. *Diabetologia*. 2017;60:1304–1313. doi: 10.1007/s00125-017-4261-z
30. Rubic T, Lametschwandtner G, Jost S, Hinteregger S, Kund J, Carballido-Perrig N, Schwarzler C, Junt T, Voshol H, Meingassner JG, et al. Triggering the succinate receptor GPR91 on dendritic cells enhances immunity. *Nat Immunol*. 2008;9:1261–1269. doi: 10.1038/ni.1657
31. Vujic A, Koo ANM, Prag HA, Krieg T. Mitochondrial redox and TCA cycle metabolite signaling in the heart. *Free Radic Biol Med*. 2021;166:287–296. doi: 10.1016/j.freeradbiomed.2021.02.041
32. Andrienko T, Pasdois P, Rossbach A, Halestrap AP. Real-time fluorescence measurements of ros and [$Ca^{2+}$] in ischemic/reperfused rat hearts: detectable increases occur only after mitochondrial pore opening and are attenuated by ischemic preconditioning. *PLoS One*. 2016;11:e0167300. doi: 10.1371/journal.pone.0167300
33. Cope DK, Impastato WK, Cohen MV, Downey JM. Volatile anesthetics protect the ischemic rabbit myocardium from infarction. *Anesthesiology*. 1997;86:699–709. doi: 10.1097/00000542-199703000-00023
34. Headrick JP, See Hoe LE, Du Toit EF, Peart JN. Opioid receptors and cardioprotection—'opioidergic conditioning' of the heart. *Br J Pharmacol*. 2015;172:2026–2050. doi: 10.1111/bph.13042
35. Molojavyi A, Preckel B, Comfere T, Mullenheim J, Thamer V, Schlack W. Effects of ketamine and its isomers on ischemic preconditioning in the isolated rat heart. *Anesthesiology*. 2001;94:623–629; discussion 625A–626A. doi: 10.1097/00000542-200104000-00016
36. Kishikawa JI, Inoue Y, Fujikawa M, Nishimura K, Nakanishi A, Tanabe T, Imamura H, Yokoyama K. General anesthetics cause mitochondrial dysfunction and reduction of intracellular ATP levels. *PLoS One*. 2018;13:e0190213. doi: 10.1371/journal.pone.0190213
37. Zielonka J, Vasquez-Vivar J, Kalyanaraman B. Detection of 2-hydroxyethidium in cellular systems: a unique marker product of superoxide and hydroethidine. *Nat Protoc*. 2008;3:8–21. doi: 10.1038/nprot.2007.473
38. Li J, Iorga A, Sharma S, Youn JY, Partow-Navid R, Umar S, Cai H, Rahman S, Eghbali M. Intralipid, a clinically safe compound, protects the heart against ischemia-reperfusion injury more efficiently than cyclosporine-A. *Anesthesiology*. 2012;117:836–846. doi: 10.1097/ALN.0b013e3182655e73
39. Robinson KM, Janes MS, Pehar M, Monette JS, Ross MF, Hagen TM, Murphy MP, Beckman JS. Selective fluorescent imaging of superoxide in vivo using ethidium-based probes. *Proc Natl Acad Sci USA*. 2006;103:15038–15043. doi: 10.1073/pnas.0601945103
40. Polster BM, Nicholls DG, Ge SX, Roelofs BA. Use of potentiometric fluorophores in the measurement of mitochondrial reactive oxygen species. *Methods Enzymol*. 2014;547:225–250. doi: 10.1016/B978-0-12-801415-8.00013-8
41. Roelofs BA, Ge SX, Studlack PE, Polster BM. Low micromolar concentrations of the superoxide probe MitoSOX uncouple neural mitochondria and inhibit complex IV. *Free Radic Biol Med*. 2015;86:250–258. doi: 10.1016/j.freeradbiomed.2015.05.032
42. Kulkarni CA, Fink BD, Gibbs BE, Chheda PR, Wu M, Sivitz WI, Kerns RJ. A novel triphenylphosphonium carrier to target mitochondria without uncoupling oxidative phosphorylation. *J Med Chem*. 2021;64:662–676. doi: 10.1021/acs.jmedchem.0c01671
43. Reily C, Mitchell T, Chacko BK, Benavides G, Murphy MP, Darley-Usmar V. Mitochondrially targeted compounds and their impact on cellular bioenergetics. *Redox Biol*. 2013;1:86–93. doi: 10.1016/j.redox.2012.11.009
44. Varadarajan SG, An J, Novalija E, Smart SC, Stowe DF. Changes in [Na(+)](i), compartmental [Ca(2+)], and NADH with dysfunction after global ischemia in intact hearts. *Am J Physiol Heart Circ Physiol*. 2001;280:H280–H293. doi: 10.1152/ajpheart.2001.280.1.H280
45. Riess ML, Camara AK, Chen Q, Novalija E, Rhodes SS, Stowe DF. Altered NADH and improved function by anesthetic and ischemic preconditioning in guinea pig intact hearts. *Am J Physiol Heart Circ Physiol*. 2002;283:H53–H60. doi: 10.1152/ajpheart.01057.2001
46. Lu LS, Liu YB, Sun CW, Lin LC, Su MJ, Wu CC. Optical mapping of myocardial reactive oxygen species production throughout the reperfusion of global ischemia. *J Biomed Opt*. 2006;11:021012. doi: 10.1117/1.2186321
47. Bauer TM, Giles AV, Sun J, Femnou A, Covian R, Murphy E, Balaban RS. Perfused murine heart optical transmission spectroscopy using optical catheter and integrating sphere: effects of ischemia/reperfusion. *Anal Biochem*. 2019;586:113443. doi: 10.1016/j.ab.2019.113443
48. Girouard SD, Pastore JM, Laurita KR, Gregory KW, Rosenbaum DS. Optical mapping in a new guinea pig model of ventricular tachycardia reveals mechanisms for multiple wavelengths in a single reentrant circuit. *Circulation*. 1996;93:603–613. doi: 10.1161/01.CIR.93.3.603
49. Wengrowski AM, Kuzmiak-Glancy S, Jaimes R III, Kay MW. NADH changes during hypoxia, ischemia, and increased work differ between isolated heart preparations. *Am J Physiol Heart Circ Physiol*. 2014;306:H529–H537. doi: 10.1152/ajpheart.00696.2013
50. Barlow CH, Harden WR III, Harken AH, Simson MB, Haselgrove JC, Chance B, O'Connor M, Austin G. Fluorescence mapping of mitochondrial redox changes in heart and brain. *Crit Care Med*. 1979;7:402–406. doi: 10.1097/00003246-197909000-00011
51. Chance B, Cohen P, Jobsis F, Schoener B. Intracellular oxidation-reduction states in vivo. *Science*. 1962;137:499–508. doi: 10.1126/science.137.3529.499
52. Ivanes F, Faccenda D, Gatliff J, Ahmed AA, Cocco S, Cheng CH, Allan E, Russell C, Duchen MR, Campanella M. The compound BTB06584 is an IF1 -dependent selective inhibitor of the mitochondrial F1 Fo-ATPase. *Br J Pharmacol*. 2014;171:4193–4206. doi: 10.1111/bph.12638
53. Faccenda D, Campanella M. Molecular regulation of the mitochondrial F(1)F(o)-ATPsynthase: physiological and pathological significance of the inhibitory factor 1 (IF(1)). *Int J Cell Biol*. 2012;2012:367934. doi: 10.1155/2012/367934
54. Honda HM, Korge P, Weiss JN. Mitochondria and ischemia/reperfusion injury. *Ann N Y Acad Sci*. 2005;1047:248–258. doi: 10.1196/annals.1341.022
55. Kanaide H, Yoshimura R, Makino N, Nakamura M. Regional myocardial function and metabolism during acute coronary artery occlusion. *Am J Physiol*. 1982;242:H980–H989. doi: 10.1152/ajpheart.1982.242.6.H980
56. Guarnieri C, Flamigni F, Caldarera CM. Role of oxygen in the cellular damage induced by re-oxygenation of hypoxic heart. *J Mol Cell Cardiol*. 1980;12:797–808. doi: 10.1016/0022-2828(80)90081-4
57. Hess ML, Manson NH. Molecular oxygen: friend and foe. The role of the oxygen free radical system in the calcium paradox, the oxygen paradox and ischemia/reperfusion injury. *J Mol Cell Cardiol*. 1984;16:969–985. doi: 10.1016/S0022-2828(84)80011-5
58. Raedschelders K, Ansley DM, Chen DD. The cellular and molecular origin of reactive oxygen species generation during myocardial ischemia and reperfusion. *Pharmacol Ther*. 2012;133:230–255. doi: 10.1016/j.pharmthera.2011.11.004
59. Brand MD, Goncalves RL, Orr AL, Vargas L, Gerencser AA, Borch Jensen M, Wang YT, Melov S, Turk CN, Matzen JT, et al. Suppressors of superoxide-$H_2O_2$ production at site IQ of mitochondrial complex I protect against stem cell hyperplasia and ischemia-reperfusion injury. *Cell Metab*. 2016;24:582–592. doi: 10.1016/j.cmet.2016.08.012
60. Valls-Lacalle L, Barba I, Miro-Casas E, Alburquerque-Bejar JJ, Ruiz-Meana M, Fuertes-Agudo M, Rodriguez-Sinovas A, Garcia-Dorado D. Succinate dehydrogenase inhibition with malonate during reperfusion reduces infarct size by preventing mitochondrial permeability transition. *Cardiovasc Res*. 2016;109:374–384. doi: 10.1093/cvr/cvv279
61. Ovens MJ, Davies AJ, Wilson MC, Murray CM, Halestrap AP. AR-C155858 is a potent inhibitor of monocarboxylate transporters MCT1 and MCT2 that binds to an intracellular site involving transmembrane helices 7-10. *Biochem J*. 2010;425:523–530. doi: 10.1042/BJ20091515
62. Zuidema MY, Zhang C. Ischemia/reperfusion injury: the role of immune cells. *World J Cardiol*. 2010;2:325–332. doi: 10.4330/wjc.v2.i10.325

63. Smiley D, Smith MA, Carreira V, Jiang M, Koch SE, Kelley M, Rubinstein J, Jones WK, Tranter M. Increased fibrosis and progression to heart failure in MRL mice following ischemia/reperfusion injury. *Cardiovasc Pathol*. 2014;23:327–334. doi: 10.1016/j.carpath.2014.06.001
64. Bonaventura A, Montecucco F, Dallegri F. Cellular recruitment in myocardial ischaemia/reperfusion injury. *Eur J Clin Invest*. 2016;46:590–601. doi: 10.1111/eci.12633
65. Chen YR, Zweier JL. Cardiac mitochondria and reactive oxygen species generation. *Circ Res*. 2014;114:524–537. doi: 10.1161/CIRCRESAHA.114.300559
66. Quinlan CL, Perevoshchikova IV, Hey-Mogensen M, Orr AL, Brand MD. Sites of reactive oxygen species generation by mitochondria oxidizing different substrates. *Redox Biol*. 2013;1:304–312. doi: 10.1016/j.redox.2013.04.005
67. Miyadera H, Shiomi K, Ui H, Yamaguchi Y, Masuma R, Tomoda H, Miyoshi H, Osanai A, Kita K, Omura S. Atpenins, potent and specific inhibitors of mitochondrial complex II (succinate-ubiquinone oxidoreductase). *Proc Natl Acad Sci USA*. 2003;100:473–477. doi: 10.1073/pnas.0237315100
68. Miyamae M, Camacho SA, Weiner MW, Figueredo VM. Attenuation of postischemic reperfusion injury is related to prevention of $[Ca^{2+}]$m overload in rat hearts. *Am J Physiol*. 1996;271:H2145–H2153. doi: 10.1152/ajpheart.1996.271.5.H2145
69. Silverman HS, Stern MD. Ionic basis of ischaemic cardiac injury: insights from cellular studies. *Cardiovasc Res*. 1994;28:581–597. doi: 10.1093/cvr/28.5.581
70. Brookes PS, Yoon Y, Robotham JL, Anders MW, Sheu SS. Calcium, ATP, and ROS: a mitochondrial love-hate triangle. *Am J Physiol Cell Physiol*. 2004;287:C817–C833. doi: 10.1152/ajpcell.00139.2004
71. Zielonka J, Srinivasan S, Hardy M, Ouari O, Lopez M, Vasquez-Vivar J, Avadhani NG, Kalyanaraman B. Cytochrome c-mediated oxidation of hydroethidine and mito-hydroethidine in mitochondria: identification of homo- and heterodimers. *Free Radic Biol Med*. 2008;44:835–846. doi: 10.1016/j.freeradbiomed.2007.11.013
72. Pak VV, Ezerina D, Lyublinskaya OG, Pedre B, Tyurin-Kuzmin PA, Mishina NM, Thauvin M, Young D, Wahni K, Martinez Gache SA, et al. Ultrasensitive genetically encoded indicator for hydrogen peroxide identifies roles for the oxidant in cell migration and mitochondrial function. *Cell Metab*. 2020;31:642–653.e646. doi: 10.1016/j.cmet.2020.02.003
73. Zhao Y, Hu Q, Cheng F, Su N, Wang A, Zou Y, Hu H, Chen X, Zhou HM, Huang X, et al. SoNar, a highly responsive $NAD^+$/NADH sensor, allows high-throughput metabolic screening of anti-tumor agents. *Cell Metab*. 2015;21:777–789. doi: 10.1016/j.cmet.2015.04.009
74. Kalinovic S, Oelze M, Kroller-Schon S, Steven S, Vujacic-Mirski K, Kvandova M, Schmal I, Al Zuabi A, Munzel T, Daiber A. Comparison of mitochondrial superoxide detection ex vivo/in vivo by mitoSOX HPLC method with classical assays in three different animal models of oxidative stress. *Antioxidants (Basel)*. 2019;8:514. doi: 10.3390/antiox8110514

# SUPPLEMENTAL MATERIAL

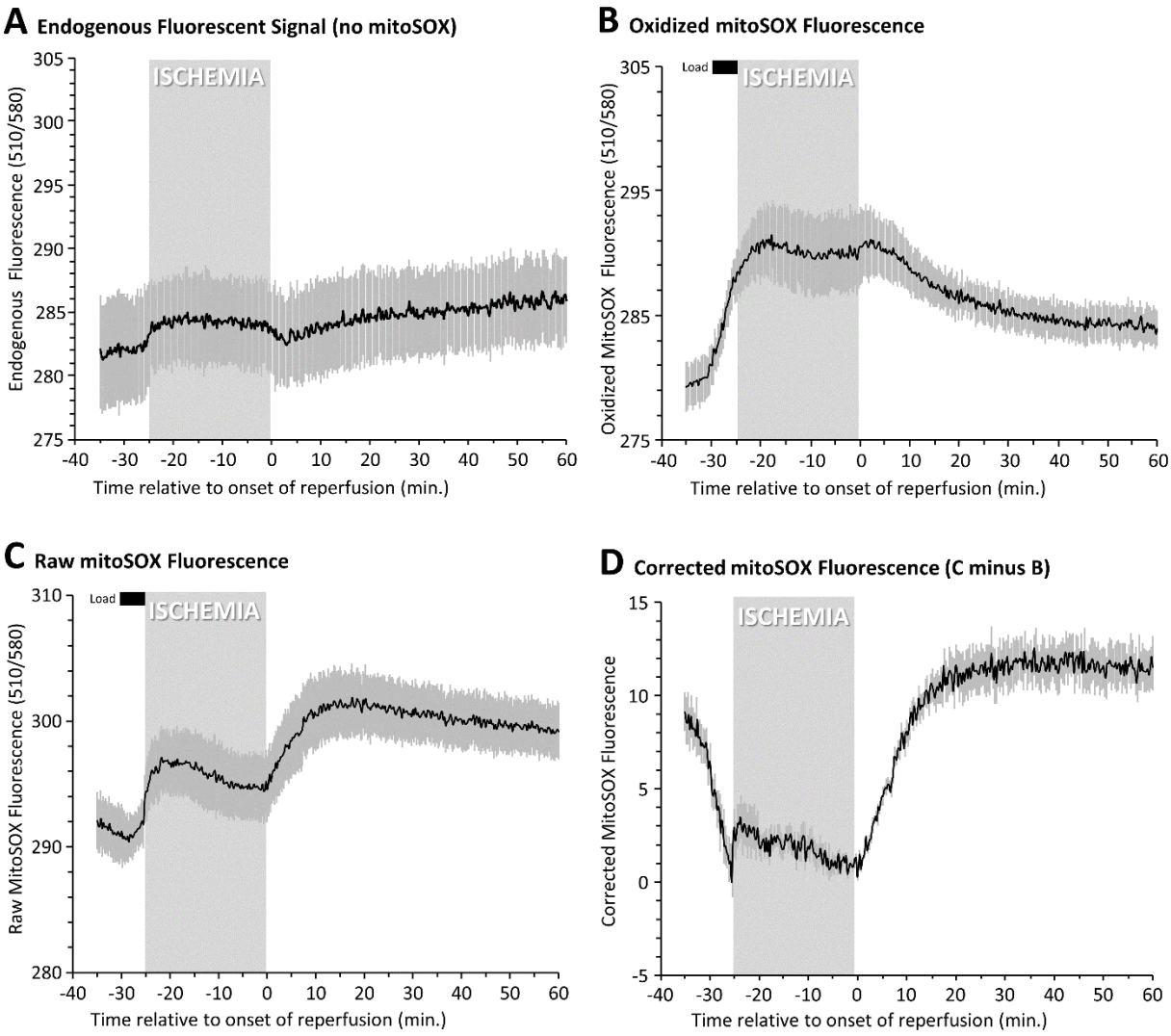


**Figure S1. Correction of mitoSOX Fluorescence Data.** Fluorescent data (510/580 nm) were obtained throughout the IR injury protocol, and were normalized as described in the methods. **(A):** Signal obtained in the absence of mitoSOX ("no probe" control). **(B):** Signal obtained in the presence of oxidized mitoSOX. 5 min. period of dye loading is indicated by the black bar. **(C):** Signal obtained in the presence of naïve mitoSOX. 5 min. period of dye loading is indicated by the black bar. **(D):** Corrected mitoSOX data, obtained by subtracting the data in panel B from those in panel C, and normalizing the signal for the 5 min. immediately prior to reperfusion, to a value of 1. All traces show means ± SEM, N= 4-6.

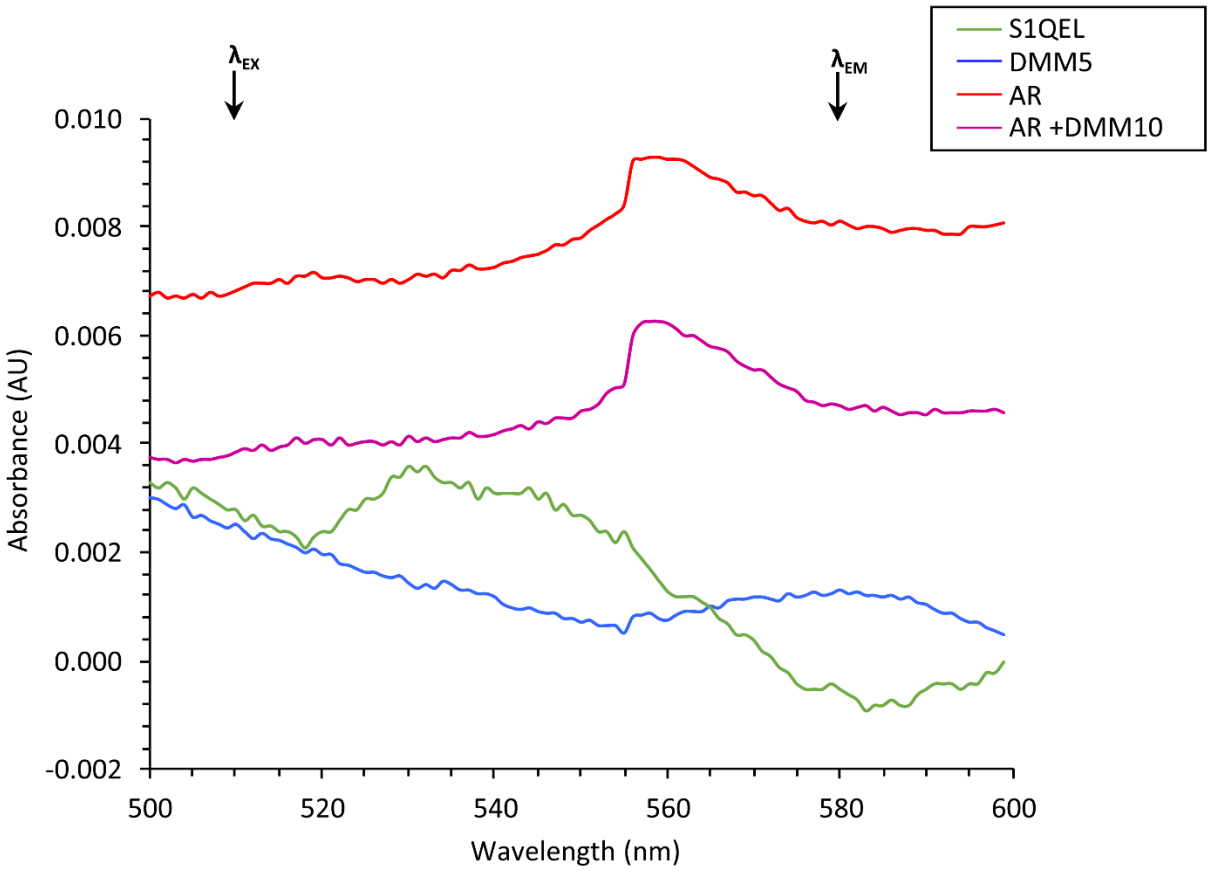


**Figure S2. Wavelength Scans for Reagents used in Perfusions.** Absorbance spectra were obtained using a Beckman DU800 UV/Vis spectrophotometer with tungsten and deuterium lamps, quartz cuvets. Graphs show difference spectra (normalized against Krebs-Henseleit buffer) for 1.6 µM S1QEL, 5 mM dimethyl malonate, 10 µM AR-C155858, or 10 µM AR-C155858 plus 10 mM DMM. Colors as per scheme in Figure 1. Excitation and emission wavelengths for mitoSOX are indicated. None of the reagents resulted in a greater than 8 milli OD unit change in absorbance at the required wavelengths.

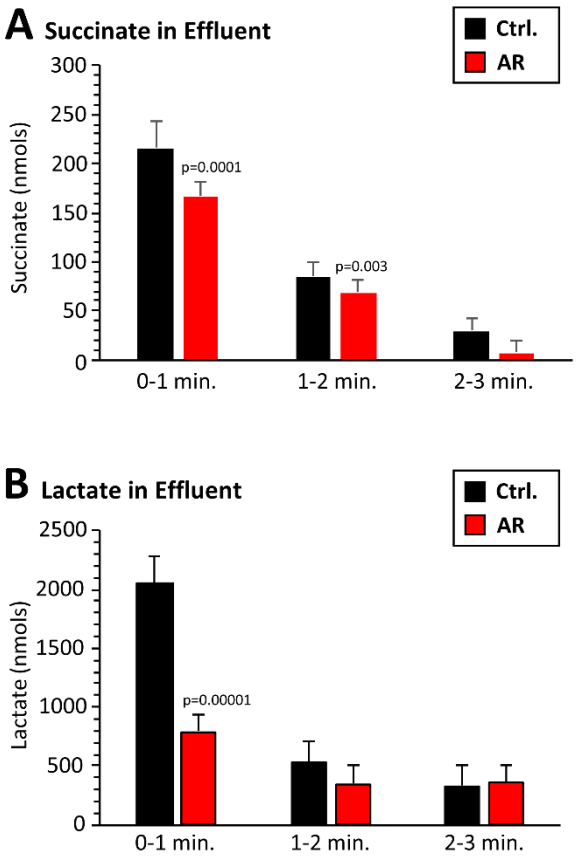


**Figure S3. HPLC Quantitation of Metabolites in Cardiac Effluent.** Cardiac perfusates (effluents) were collected in 1 ml aliquots for the first 3 min. of reperfusion, from control hearts or those treated with AR. Perfusion was at a rate of 4 ml/min, so each minute yielded 4 ml of perfusate. Metabolites were analyzed by HPLC with UV/Vis detection as described [1]. Data for **(A):** succinate and **(B):** lactate, are shown as means ± SEM, N=10. p-values above bars (Tukey's HSD test) denote significance between control vs. AR groups.

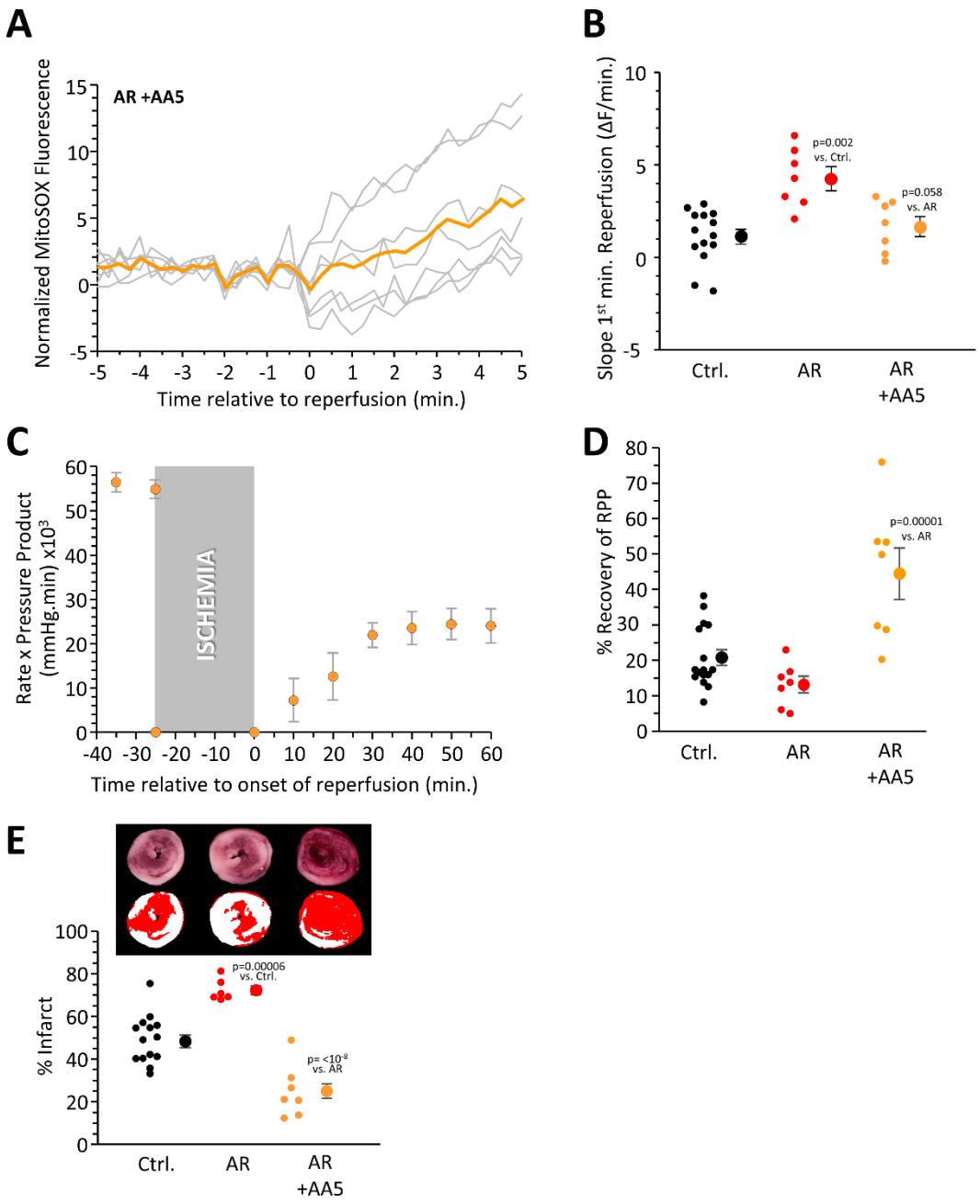


**Figure S4. Data for Atpenin A5.** Hearts were treated with AR, or AR plus 100 nM AA5 (see Figure 1 scheme). **(A):** mitoSOX signal upon reperfusion. Gray traces show individual data, with averages shown as bold line. **(B):** Quantitation of mitoSOX slope. Data for control and AR conditions are as per Figure 3F. **(C):** Cardiac function. **(D):** Quantitation of cardiac functional recovery. Data for control and AR conditions are as per Figure 4B. **(E):** Infarct size. Data for control and AR are as per Figure 4C. N for each condition (mitoSOX measurements or cardiac parameters) is indicated by the number of individual data points in panels B and D. Data are means ± SEM. p values (ANOVA followed by Tukey's HSD test) for differences between groups are denoted.

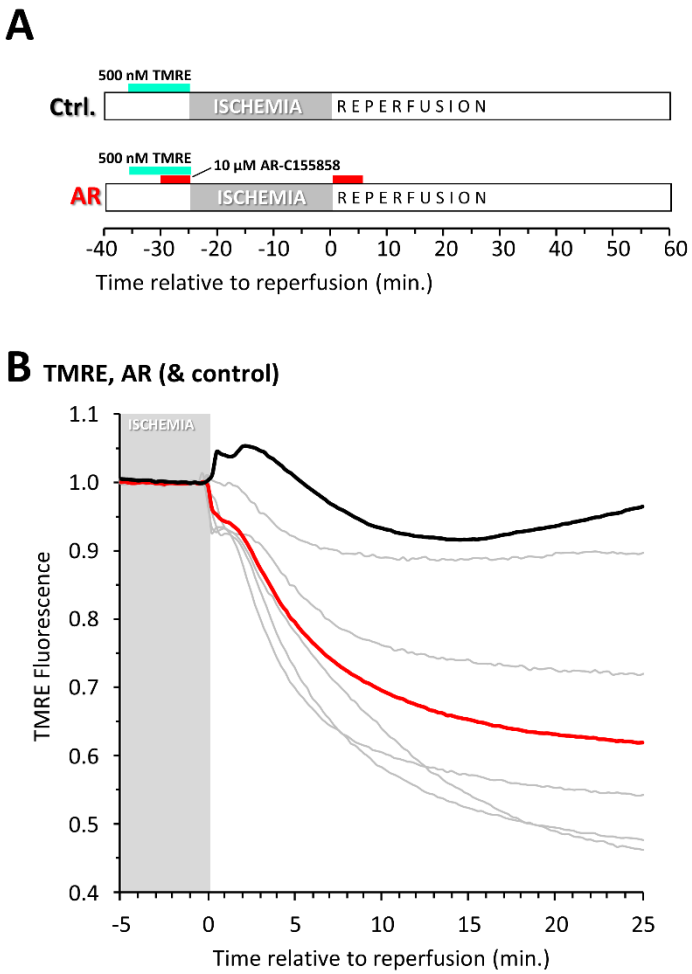


**Figure S5. Impact of MCT-1 Inhibition on PT Pore Opening During IR. (A):** Schematic showing perfusion conditions. Where indicated, TMRE ($\Delta\Psi_m$ indicator) and AR-C155858 (MCT-1 inhibitor) were administered at the listed concentrations. **(B):** Normalized TMRE fluorescence during early reperfusion under control or AR condition. The last 5 min. of the ischemic period is indicated. Gray traces show individual data, with the average of the AR condition shown in bold red. Average control data from Figure 7D of the main manuscript are shown in black.